STRUCTURAL BIOLOGY COMMUNICATIONS

ISSN 2053-230X

Structure of α-carbonic anhydrase from the human pathogen *Helicobacter pylori*

Maria Elena Compostella, Paola Berto, Francesca Vallese and Giuseppe Zanotti*

Department of Biomedical Sciences, University of Padua, Via Ugo Bassi 58/B, 35131 Padua, Italy. *Correspondence e-mail: giuseppe.zanotti@unipd.it

Received 12 March 2015
Accepted 31 May 2015

Edited by N. Sträter, University of Leipzig, Germany

Keywords: *Helicobacter pylori*; carbonic anhydrase; metalloproteins; periplasmic protein.

PDB reference: α-carbonic anhydrase from *H. pylori*, 4xfw

Supporting information: this article has supporting information at journals.iucr.org/f

The crystal structure of α-carbonic anhydrase, an enzyme present in the periplasm of *Helicobacter pylori*, a bacterium that affects humans and that is responsible for several gastric pathologies, is described. Two enzyme monomers are present in the asymmetric unit of the monoclinic space group $P2_1$, forming a dimer in the crystal. Despite the similarity of the enzyme structure to those of orthologues from other species, the *H. pylori* protein has adopted peculiar features in order to allow the bacterium to survive in the difficult environment of the human stomach. In particular, the crystal structure shows how the bacterium has corrected for the mutation of an essential amino acid important for catalysis using a negative ion from the medium and how it localizes close to the inner membrane in the periplasm. Since carbonic anhydrase is essential for the bacterial colonization of the host, it is a potential target for antibiotic drugs. The definition of the shape of the active-site entrance and cavity constitutes a basis for the design of specific inhibitors.

1. Introduction

Helicobacter pylori, a Gram-negative pathogen responsible for several gastric pathologies, including gastritis, peptic ulcers, gastric adenocarcinoma and MALT lymphoma (Suerbaum & Michetti, 2002; Kusters *et al.*, 2006), relies on several factors in order to survive in the acidic environment of the stomach (Foster, 1999; Wen *et al.*, 2003; Zanotti & Cendron, 2010). Particularly important in this respect are the enzymes urease (Huynh & Grinstein, 2007) and carbonic anhydrase (Marcus *et al.*, 2005).

Carbonic anhydrase (CA; carbonate hydro-lyase; EC 4.2.1.1) is a Zn^{2+}-containing enzyme that catalyzes the reversible conversion of carbon dioxide to bicarbonate (Tripp *et al.*, 2001). Since CA plays several important physiological roles in humans and is ubiquitous in many tissues, it is considered to be an attractive pharmacological target. Its inhibitors are clinically used to treat diseases as different as glaucoma, convulsions and obesity; the enzyme is also a tumour marker (Supuran & Scozzafava, 2007; Gilmour, 2010). The mammalian CAs, which include 16 different isoforms, have been extensively characterized (for a review, see, for example, Lindskog, 1997); the catalytic mechanism has been thoroughly described (Boone *et al.*, 2014) and structural studies have led to the deposition of 477 crystal structures in the Protein Data Bank (http://www.pdb.org), either in the native form or with inhibitors or ligands bound.

In mammals only one class of CA is present, named α-CA, whilst five different classes of the enzyme, α-CA, β-CA, γ-CA, δ-CA and ζ-CA, have been found in bacteria, archaea and diatoms. Very recently, a new carbonic anhydrase family, named η-CA, has been identified (Del Prete *et al.*, 2014).

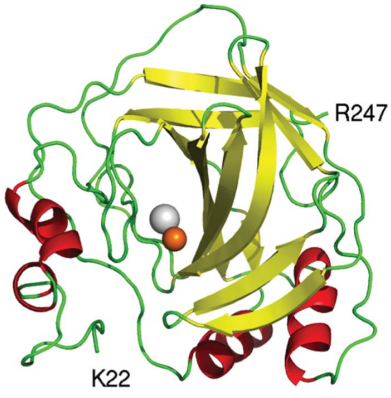

Table 1
Macromolecule-production information.

Source organism	*H. pylori*
DNA source	*H. pylori* strain G27
Forward primer	5′-CAT CAT CAC CAC CAT CAC GAA AAC CTG TAT TTT CAG GGA AAA TGG GAT TAT AAA AAT AAA GAA-3′
Reverse primer	5′-GTG GCG GCC GCT CTA TTA GCG GGT CTC AGC TGA-3′
Cloning vector	pETite N-His Kan Vector (Lucigen)
Expression vector	pETite N-His Kan Vector (Lucigen)
Expression host	*E. coli* BL21 (DE3)
Complete amino-acid sequence of the construct produced	HHHHHHENLYFQGKWDYKNKENGPHRWDKLHKDF-EVCKSGKSQSPINIEHYYHTQDKADLQFKYAA-SKPKAVFFTHHTLKASFEPTNHINYRGHDYVL-DNVHFHAPMEFLINNKTRPLSAHFVHKDAKGR-LLVLAIGFEEGKENPNLDPILEGIQKKQNFKE-VALDAFLPKSINYYHFNGSLTAPPCTEGVAWF-VVEEPLEVSAKQLAEIKKRMKNSPNQRPVQPD-YNTVIIKRSAETR

Despite the fact that these classes do not share sequence or structural similarity, their active-site structure and catalytic mechanism are common, a clear example of convergent evolution (Liljas & Laurberg, 2000; Tripp *et al.*, 2001). Since they are often essential for the survival of the organism, bacterial CAs are considered to be potential pharmacological targets for antibacterial drugs (Supuran, 2011). CAs from bacteria and archaea have been less studied structurally than their human counterpart; the crystal structures of CAs of various classes from 11 different bacteria and two archaea have been determined to date (Supplementary Table S1).

Two different carbonic anhydrases are coded by the genome of *H. pylori*: the periplasmic α-carbonic anhydrase and the cytoplasmic β-carbonic anhydrase (named HP1186 and HP0004, respectively, in strain 26695). The role of α-CA in *H. pylori* (HpαCA) is fundamental in buffering the pH of the periplasm, since when the ammonia and carbon dioxide produced by urease in the cytoplasm diffuse back, at least partially, into the periplasmic space, this catalyzes the conversion of CO_2 to HCO_3^-. It is reasonable to assume that β-CA in the cytoplasm plays the same role for the CO_2 molecules that do not freely diffuse out of the inner membrane. HpαCA expression has been shown to be induced under acidic conditions by a two-component (ArsRS) system (Wen *et al.*, 2007). HpαCA has been shown to be essential for acid acclimatization (Marcus *et al.*, 2005) and some CA-defective *H. pylori* mutants exhibited only reduced stomach colonization *in vivo*, despite the fact that CA does not seem to have an effect on urease activity *in vitro* (Bury-Moné *et al.*, 2008). Both HpCAs have been proposed as alternative possible therapeutic targets for the treatment of patients infected by drug-resistant strains of the bacterium, and several inhibitors have been identified (Nishimori, Minakuchi *et al.*, 2006; Nishimori, Vullo *et al.*, 2006; Nishimori *et al.*, 2007). In this context, the design of selective inhibitors for HpαCA could help to better clarify the effective role played by this enzyme in the control of pH and could eventually open the way to improved classes of therapeutics against the bacterium. The crystallization of HpαCA with acetazolamide in a orthorhombic crystal form (Modak *et al.*, 2013) has been published and its structure complexed with the clinically used compound sulfonamide has recently been published (Modakh *et al.*, 2015). In this paper, the crystal structure of HpαCA is presented and the possible implications for its function are discussed.

Table 2
Crystallization.

Method	Sitting-drop vapour diffusion
Plate type	SWISSCI MRC two-drop crystallization plate
Temperature (K)	277
Protein concentration (mg ml^{-1})	20
Buffer composition of protein solution	30 m*M* Tris–HCl pH 8.0
Composition of reservoir solution	0.2 *M* sodium nitrate, 0.1 *M* bis-tris propane pH 8.5, 20%(*w*/*v*) PEG 3350
Volume of drop (nl)	800
Volume of reservoir (µl)	70

2. Materials and methods

2.1. Macromolecule production

The coding sequence for the α-carbonic anhydrase gene (HPG27_1129) was PCR-amplified from genomic *H. pylori* DNA (strain G27) using Phusion High-Fidelity DNA Polymerase (New England Biolabs). Since the full-length protein is toxic to *Escherichia coli*, the N-terminal export signal sequence was excluded and an N-terminal 6×His tag and a TEV proteolysis site were included (Table 1).

E. coli BL21 (DE3) cells were grown in Luria–Bertani medium. Expression was induced by adding 0.5 m*M* isopropyl β-D-1-thiogalactopyranoside (IPTG) to the medium and was continued for 5 h at 30°C with constant shaking. The cells were resuspended in 50 m*M* Tris–HCl pH 7, 150 m*M* NaCl, 5 m*M* imidazole supplemented with protease inhibitors (1 m*M* PMSF, 15 µ*M* aprotinin, 1 m*M* leupeptin) and lysed using a One Shot Cell disruption system (Constant Systems Ltd). The lysate was centrifuged at 18 000 rev min^{-1} for 20 min at 4°C to separate the supernatant from the insoluble fraction. The soluble fraction was loaded onto a HisTrap HP Ni–NTA column (GE Healthcare) pre-equilibrated with lysis buffer. The column was extensively washed with buffer *A* and the protein was eluted using a linear gradient from 350 to 500 m*M* imidazole. The protein eluted as a single species and was further purified by buffer exchange using a PD-10 desalting column (GE Healthcare) equilibrated with a buffer consisting of 50 m*M* Tris–HCl pH 7, 150 m*M* NaCl. The His tag was removed by incubation with TEV protease (Sigma–Aldrich) in a 1:100 ratio overnight at 30°C. The reaction mixture was buffer-exchanged with buffer consisting of 50 m*M* Tris–HCl pH 8, 500 m*M* NaCl, 15 m*M* imidazole, 1%(*v*/*v*) glycerol. The cleaved protein was isolated as an unbound sample by loading it onto an Ni Sepharose 6 Fast Flow column (GE Healthcare) equilibrated with buffer. The protein was buffer-exchanged into 30 m*M* Tris–HCl pH 8, concentrated to 20 mg ml^{-1} using

Table 3
Data collection and processing.

Values in parentheses are for the outer shell.

Diffraction source	Beamline PXIII, SLS
Wavelength (Å)	1.00
Temperature (K)	100
Detector	Pilatus 2M
Rotation range per image (°)	0.1
Total rotation range (°)	180
Exposure time per image (s)	0.1
Space group	$P2_1$
a, b, c (Å)	44.906, 95.905, 53.318
α, β, γ (°)	90, 92.92, 90
Resolution range (Å)	47.961–1.517 (1.60–1.517)
Total No. of reflections	229967
No. of unique reflections	69653 (8705)
Completeness (%)	96.7 (85.8)
Multiplicity	3.3 (3.0)
$\langle I/\sigma(I)\rangle$	3.3 (3.0)
$R_{\rm sym}$	0.037 (0.382)
$R_{\rm p.i.m.}$	0.024 (0.256)
Overall B factor from Wilson plot (Å^2)	16.97

a Vivaspin 20 5000 Da cutoff centrifugal concentrator (Sartorius) and stored at −20°C for crystallization trials.

2.2. Crystallization

The purified protein was concentrated to 20 mg ml^{-1} and used in crystallization tests, which were partially automated using an Oryx8 crystallization robot (Douglas Instruments, UK). The best crystals were obtained at 4°C by the sitting-drop vapour-diffusion technique using a solution consisting of 0.2 *M* sodium nitrate, 0.1 *M* bis-tris propane pH 8.5, 20%(*w*/*v*) PEG 3350 as a precipitant (The PACT Suite solution No. 89, Qiagen; Table 2).

2.3. Data collection and processing

Diffraction data were measured on the PXIII beamline at the SLS synchrotron, Villigen, Switzerland. The crystal was found to belong to the monoclinic space group $P2_1$, with unit-cell parameters $a = 44.906$, $b = 95.905$, $c = 53.318$ Å, $\beta = 92.92°$. Two molecules are present in the asymmetric unit, corresponding to a $V_{\rm M}$ of 2.03 Å^3 Da^{-1} and an approximate solvent content of 39%. All data sets were indexed and integrated with *XDS* (Kabsch, 2010) and merged and scaled with *SCALA* (Evans, 2006) as contained in the *CCP*4 crystallographic package (Winn *et al.*, 2011; Table 3).

2.4. Structure solution and refinement

The structure was solved by molecular replacement using *MOLREP* (Vagin & Teplyakov, 2010), starting from a model built using the *SWISS-MODEL* server (Biasini *et al.*, 2014) from PDB entry 4g7a (Di Fiore *et al.*, 2013). The rebuilding procedure available in the *PHENIX* package was used to rebuild the model, which was subsequently checked and adjusted with *Coot* (Emsley *et al.*, 2010). Refinement was continued with *PHENIX* (Adams *et al.*, 2010). The final statistics of the refinement are summarized in Table 4.

Table 4
Structure solution and refinement.

Resolution range (Å)	47.96–1.52
Completeness (%)	96.7
σ Cutoff	0
No. of reflections, working set	63791
No. of reflections, test set	3384
Final $R_{\rm cryst}$	0.1696
Final $R_{\rm free}$	0.1984
No. of non-H atoms	
Total	4396
Protein	3721
Ions	4
Others	8
Water	662
R.m.s. deviations	
Bonds (Å)	0.007
Angles (°)	1.15
Average B factor (Å^2)	22.6
Ramachandran plot	
Most favoured (%)	96.0
Allowed (%)	3.6

3. Results and discussion

3.1. Overall fold of the enzyme

The asymmetric unit of the HpαCA crystal contains two monomers. Their structure is essentially the same (r.m.s.d. of 0.61 Å), with the exception of the long stretch from residues 61 to 68. Each monomer includes 226 residues (22–247; Fig. 1*a*; the first 21 amino acids were not included in the gene cloned, since they are predicted to correspond to a signal sequence for export into the periplasmic space of the bacterium). The entire polypeptide chain is very well defined in the electron-density map, with the exception of amino acids 163–167 of monomer *B*, a stretch that is exposed to the solvent and is far away from the active site and from the contact region with the other monomer (see below). The fold of the HpαCA monomer corresponds to that of the classical α-CA, characterized by a central ten-stranded β-sheet surrounded by three α-helices and by the remainder of the protein chain (Fig. 2*a*). One layer of the twisted β-sheet along with another portion of the polypeptide chain defines a conical-shaped cavity hosting a Zn^{2+} ion at the bottom. The latter defines the active site of the enzyme. The structure of the monomer is stabilized by an intramolecular disulfide bond (Cys45–Cys195) that is conserved in most CA structures (Di Fiore *et al.*, 2013). Since this disulfide bond connects the N-terminus to a loop (residues 192–195) that surrounds the entrance of the catalytic site cavity, it is tempting to speculate that its function is to keep the cavity well opened in order to favour entrance of the substrate.

3.2. Protein dimerization

The two monomers in the asymmetric unit (Fig. 2*b*) are related each other by a rotation axis of 177°. The dimer is stabilized mostly by hydrophilic interactions, in particular by the formation of 18 hydrogen bonds (Supplementary Table S2) between protein atoms. Other hydrophilic interactions are mediated by solvent molecules. The surface concealed after formation of the dimer is 1226 Å^2 per monomer, corre-

sponding to about 11% of the total surface of the monomer. This value is relatively low and analysis with *PISA* (Krissinel & Henrick, 2007) assigns quite a low score (0.123) to the dimer formation, suggesting that this interface may play only an auxiliary role in dimer formation. A size-exclusion chromatography experiment (Fig. 1*b*) confirmed that the enzyme is present as a monomeric species in solution. Altogether, these data suggest that the dimer that we observe is the result of crystal packing and that the physiological state of HpαCA is monomeric, analogously to all mammalian α-CAs. Nevertheless, it is surprising that the dimer we observe is the same dimer as found in the α-CAs from the other bacteria *Sulfurihydrogenibium yellowstonense* (Di Fiore *et al.*, 2013) and *Neisseria gonorrhoeae* (Huang *et al.*, 1998) and in the dimer of the tetrameric *Thermovibrio ammonificans* α-CA (James *et al.*, 2014). This occurs despite the regions involved in the dimerization surface not being particularly conserved. Since the interaction surface between the two monomers is essentially hydrophilic, the equilibrium between monomer and dimer possibly depends on the environmental conditions (ionic strength, pH), which in the case of the *H. pylori* periplasm can change significantly according to the pH of the host stomach. Moreover, the two active sites in the dimer are quite distant and independent, and dimerization does not affect the entrance to the two binding sites.

3.3. The active site

The Zn^{2+} ion present in the active site of HpαCA presents a slightly distorted trigonal bipyramidal coordination: the five ligands are the three N atoms of three histidine residues conserved in all other α-CAs for which structures have been determined to date and two solvent molecules (Fig. 2*c*). Coordination distances for the Zn^{2+} ion range from 2.14 to 2.19 Å in the two monomers, and from 2.12 to 2.30 Å for the solvent O atoms. The Zn^{2+} coordination in other bacterial α-CAs involves the same three histidines in all cases and varies from trigonal bipyramidal to tetrahedral according to the ligand bound. Another two important residues in the vicinity of the active site, His191 and Glu116, are conserved in several

```
B5Z8I0 1   ---MK-------KTFLIALALTASLIGAENAKWDYKNKENGPHRWDKLHKDFEVCKSGKSQSPINIEHYYHTQDK-ADLQFKYAASKPKAVFFTHHTLKASFE-PTNHINYRGHDYVLDN  108
B2V8E3 1   ---MRKIL--ISAVLVLS----SISISFAEHEWSYEG-EKGPEHWAQLKPEFFWCKL-KNQSPINIDKKYKVKANLPKLNLYYKTAKESEVVNNGHTIQINIK-EDNTLNYLGEKYQLKQ  108
E8T502 1   ---MKRVLVTLGAV----AALATGAVAGGGAHWGYSG-SIGPEHWGDLSPEYLMCKIGKNQSPIDINSADAVKACLAPVSVYYVSD-AKYVVNNGHTIKVVMG-GRGYVVVDGKRFYLKQ  110
Q50940 1   MPRFPRTLPRLTAVLLLACTAFSAAAHGNHTHWGYTG-HDSPESWGNLSEEFRLCSTGKNQSPVNITET--VSGKLPAIKVNYKPS-MVDVENNGHTIQVNYPEGGNTLTVNGRTYTLKQ  116
                 :         .         :        .* *     .*. * .*  ::  *.  *.***::*     ..     :.. *       *  . **::          :   *. : *.:
B5Z8I0 109 VHFHAPMEFLINNKTRPLSAHFVHKDAKGRLLVLAIGFEEGKENPNLDPILEGIQKKQ-----NFKEVALDAFLPKSINYYHFNGSLTAPPCTEGVAWFVVEEPLEVSAKQLAEIKKRMK  223
B2V8E3 109 FHFHTPSEHTIEKKSYPLEIHFVHKTEDGKILVVGVMAKLGKTNKELDKILNVAPAEEGEK-ILDKNLNLNNLIPKDKRYMTYSGSLTTPPCTEGVRWIVLKKPISISKQQLEKLKSVM-  226
E8T502 111 FHFHAPSEHTVNGKHYPFEAHFVHLDKNGNITVLGVFFKVGKENPELEKVWRVMPEEPGQKRHLTARIDPEKLLPENRDYYRYSGSLTTPPCSEGVRWIVFKEPVEMSREQLEKFRKVM-  229
Q50940 117 FHFHVPSENQIKGRTFPMEAHFVHLDENKQPLVLAVLYEAGKTNGRLSSIWNVMPMTAGKV-KLNQPFDASTLLPKRLKYYRFAGSLTTPPCTEGVSWLVLKTYDHIDQAQAEKFTRAV-  234
          .***.* *  :: :  *:. ****   . .  *:.:  : ** * .*. : .              .  . ::*:   *  : ****:***:*** *:*.:    :.  *  ::   :

B5Z8I0 224 NSPNQRPVQPDYNTVIIKRSAETR  247
B2V8E3 227 VNPNNRPVQEINSRWIIEGF----  246
E8T502 230 GFDNNRPVQPLNARKVMK------  247
Q50940 235 GSENNRPVQPLNARVVIE------  252
              *:****      :::
```

(*a*)

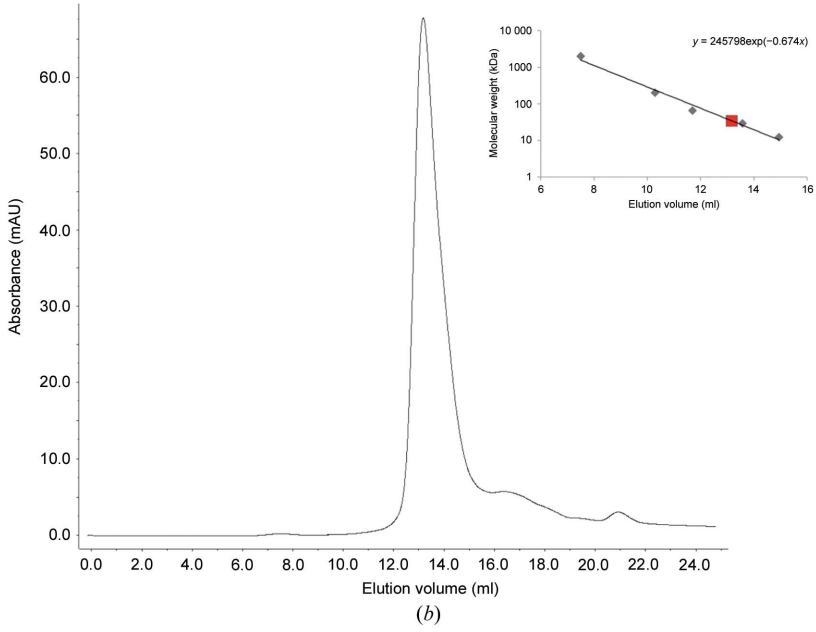

(*b*)

Figure 1
(*a*) Sequence alignment of HPαCA (B5Z8IO) with α-CA from *S. yellowstonense* (B2V8E3), *T. ammonificans* (E8T502) and *N. gonorrhoeae* (Q50940). Red, yellow and pale green backgrounds denote the residues involved in the binding of Zn^{2+}, in the conical surface of the active-site cavity and in the areas of contact in the dimer, respectively. (*b*) A gel-filtration experiment showing that the apparent molecular mass of HpαCA (red square) is about 34 000 Da, which is slightly larger than the theoretical calculated mass (26 165.7 Da) but significantly smaller than that of a dimer. The small grey square close to it corresponds to bovine α-CA.

α-CAs. The former interacts with one of the two solvent molecules that coordinate the Zn^{2+} ion, while the latter does not form any significant interactions with active-site residues in the HpαCA structure, but its negative charge is possibly fundamental to balance the global positive charge of the active site or to orient the substrate (Vullo *et al.*, 2013).

A significant difference of HpαCA with respect to the other bacterial α-CAs is represented by the environment of the active site. In all of them one of the histidines (corresponding to His129 in HpαCA) interacts with a conserved glutamic acid (position 127 in HpαCA), the negative charge of which partially neutralizes the positive charge of the histidine–Zn^{2+} complex and possibly stabilizes it. In the structure of HpαCA, amino acid 127 is a serine and an atom heavier than a water molecule is present in the position occupied by the glutamate carboxylic group in the other bacterial α-CAs. This atom interacts with $N^{\varepsilon 2}$ of His129 (at a distance of 3.11 Å) and O^{γ} of Ser127 (at a distance of 3.15–3.16 Å). It is reasonable to assume that this atom must be negatively charged to compensate for the absence of the glutamate in this position. An anomalous Fourier difference map with data measured at 1.000 Å wavelength presents a large peak (about 20σ) corresponding to the Zn^{2+} position and a smaller peak (about 5σ) corresponding to this unknown atomic species (Fig. 2*c*). This value corresponds to that for the S atoms of methionines and cysteines visible in our map. At this wavelength the f'' values for Zn^{2+} and S are 2.6 e and 0.265 e, respectively. The only monoatomic anion present in solution is Cl^-, the f'' value of which is 0.321 e, a value close to that of S. This strongly supports the presence of a chloride ion at this position. The latter would compensate for the absence of the negative charge of the glutamate.

3.4. Comparison with other α-CA structures

The overall architecture of HpαCA is quite similar to that of α-CAs from other bacteria: superposition of the corresponding C^{α} atoms of one monomer with those of the enzyme with the most similar amino-acid sequence, that from *S. yellowstonense* (PDB entry 4g7a; Di Fiore *et al.*, 2013), which presents 39% identity to our enzyme, gives an r.m.s.d. of 1.49 Å for 224 residues; on superposition with *T. ammonificans* α-CA (37% sequence identity; PDB entry 4coq; James *et al.*, 2014) the r.m.s.d. is 1.33 Å for 211 amino acids and with *N. gonorrhoeae* α-CA (36% identity; PDB entry 1kop; Huang *et al.*, 1998) the r.m.s.d. is 1.57 Å for 212 residues.

Some structural differences among α-CAs from different bacteria are possibly represented by the entrance to the active site and by the surface of the conical cavity that gives access to the active site, as discussed in detail by De Simone *et al.*

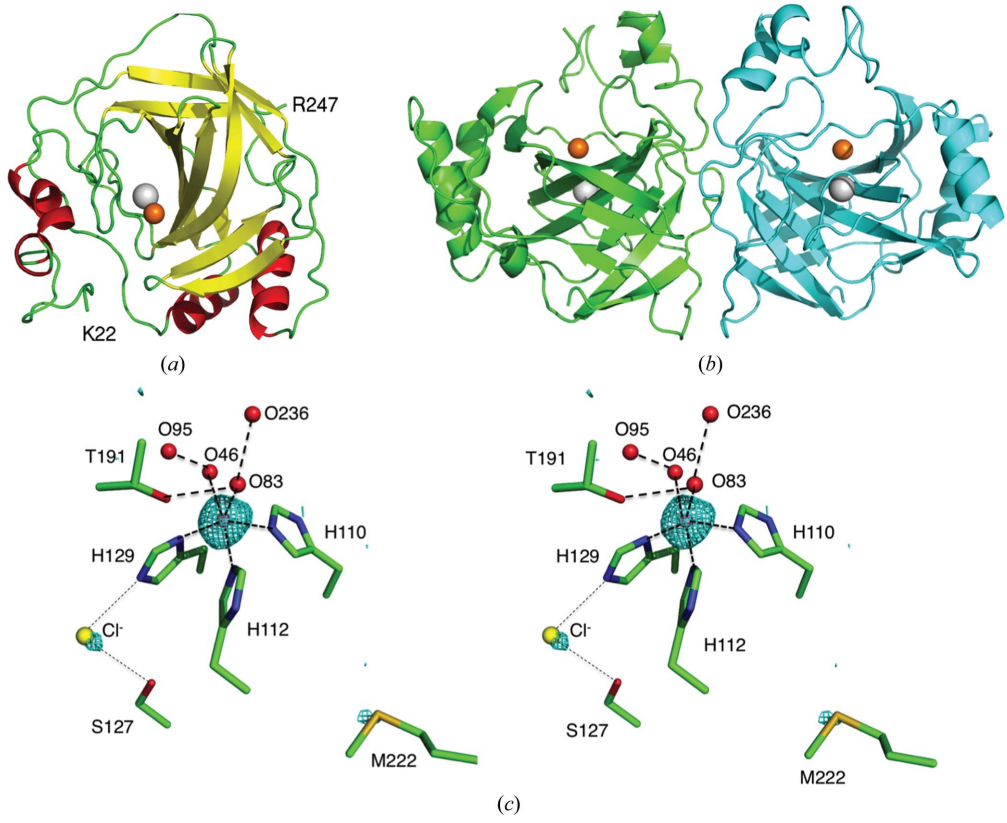

Figure 2
(*a*) Cartoon view of the monomer of HpαCA, coloured according to secondary-structure element. The Zn^{2+} and Cl^- ions are shown as orange and yellow spheres, respectively. (*b*) The HpαCA dimer present in the asymmetric unit of the crystal. A molecular twofold axis runs approximately vertically in the plane of the paper. (*c*) Stereographic view of the enzyme active site, showing the Zn^{2+} ion coordinated by three histidine residues and two solvent molecules. A Cl^- ion interacting with His129 is shown as a yellow sphere. The cyan grid represents the anomalous difference map contoured at a 5σ contour level. The position of the Met222 side chain is also shown for comparison.

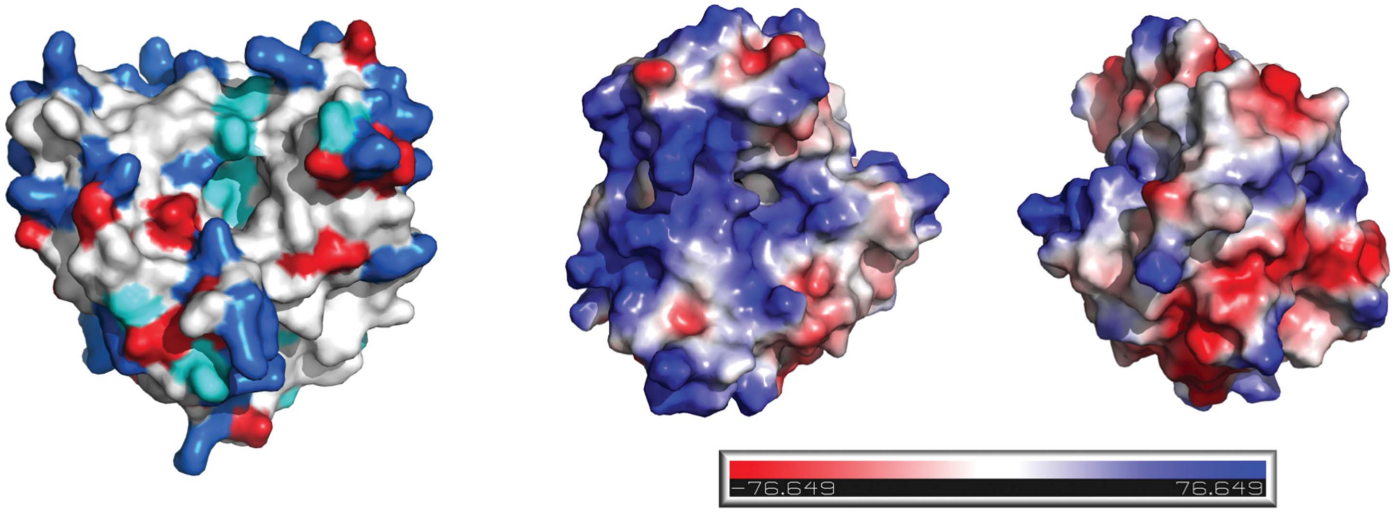

(*a*) (*b*)

Figure 3
(*a*) Surface of the HpαCA monomer. Potentially charged residues are coloured blue (Arg and Lys), red (Glu and Asp) and cyan (His). The bottom of the central cavity in the centre appears in cyan owing to the presence of the three histidine residues that coordinate the Zn^{2+}. (*b*) Qualitative electrostatic surface of the HpαCA monomer. On the left it is possible to observe the access to the active site, whilst on the right the molecule is rotated 180° in the vertical direction.

(2013). The residues lining the surface of the cavity are highlighted in Fig. 1(*a*) by a yellow background. In Fig. 3(*a*), in which residues are coloured according to their potential charge, it is possible to see that half of the entrance of the active-site cavity is charged, with a prevalence of positive charges, in particular if the histidine is protonated, whilst the other half is neutral and is mostly hydrophobic.

3.5. Localization

HpαCA has been detected bound to the inner membrane of the periplasmic space and was not found in the soluble fraction in a Western blot experiment (Marcus *et al.*, 2005). The crystal structure presented in this paper confirms that it is a soluble protein and its surface presents several positively and negatively charged residues (Fig. 3*b*). A qualitative electrostatic potential calculation indicates that positive electrostatic potentials are prevalent on the protein surface, in line with an isoelectric point of 9.1 as estimated from the amino-acid sequence. An analysis of the distribution of these charges shows that positive potential is mostly located on the face of the protein containing the opening of the active-site cavity, whilst on the rest of the surface positive and negative potentials are more randomly distributed. We can hypothesize that the positive surface of HpαCA serves to interact with the negatively charged phospholipids of the membrane. If this is true then the enzyme would present the active-site entrance roughly oriented towards the membrane in such a way that when CO_2 diffuses from the cytoplasm the enzyme could capture the gas directly as soon as it flows through the membrane.

4. Conclusion

As expected, the crystal structure of HpαCA shares many features with other members of the same family, but has some specificities that makes the crystal structure interesting. In particular, it shows the elegant way that *H. pylori* has solved the problem of the absence of a negatively charged side chain at position 127 through the use of an anion from the external medium. The crystal structure also suggests how the enzyme can localize close to the inner membrane of the bacterium, and this is coherent with the function of the enzyme in processing carbon dioxide diffusing from the cytoplasm through the membrane. Finally, the definition of the details of the shape of the active-site entrance and cavity may constitute a basis for the design of inhibitors specific for this bacterium.

Acknowledgements

We thank the staff of beamline PXIII at the Swiss Light Source (SLS), Villigen (Switzerland) for technical assistance during data collection and Laura Cendron for discussions and suggestions. The research leading to these results received funding from the European Community's Seventh Framework Program (FP7/2007-2013) under grant agreement No. 283570 (for BioStruct-X). This work was supported by the University of Padua and by PRIN 2010-2011 (MIUR) 'Unraveling structural and functional determinants behind *Helicobacter pylori* pathogenesis and persistence'.

References

Adams, P. D. *et al.* (2010). *Acta Cryst.* D**66**, 213–221.
Biasini, M., Bienert, S., Waterhouse, A., Arnold, K., Studer, G., Schmidt, T., Kiefer, F., Cassarino, T. G., Bertoni, M., Bordoli, L. & Schwede, T. (2014). *Nucleic Acids Res.* **42**, W252–W258.
Boone, C. D., Pinard, M., McKenna, R. & Silverman, D. (2014). *Subcell. Biochem.* **75**, 31–52.
Bury-Moné, S., Mendz, G. L., Ball, G. E., Thibonnier, M., Stingl, K., Ecobichon, C., Avé, P., Huerre, M., Labigne, A., Thiberge, J.-M. & De Reuse, H. (2008). *Infect. Immun.* **76**, 497–509.

Del Prete, S., Vullo, D., Fisher, G. M., Andrews, K. T., Poulsen, S.-A., Capasso, C. & Supuran, C. T. (2014). *Bioorg. Med. Chem. Lett.* **24**, 4389–4396.
De Simone, G., Alterio, V. & Supuran, C. T. (2013). *Exp. Opin. Drug. Discov.* **8**, 793–810.
Di Fiore, A., Capasso, C., De Luca, V., Monti, S. M., Carginale, V., Supuran, C. T., Scozzafava, A., Pedone, C., Rossi, M. & De Simone, G. (2013). *Acta Cryst.* D**69**, 1150–1159.
Emsley, P., Lohkamp, B., Scott, W. G. & Cowtan, K. (2010). *Acta Cryst.* D**66**, 486–501.
Evans, P. (2006). *Acta Cryst.* D**62**, 72–82.
Foster, J. (1999). *Curr. Opin. Microbiol.* **2**, 170–174.
Gilmour, K. M. (2010). *Comp. Biochem. Physiol. A Mol. Integr. Physiol.* **157**, 193–197.
Huang, S., Xue, Y., Sauer-Eriksson, E., Chirica, L., Lindskog, S. & Jonsson, B. H. (1998). *J. Mol. Biol.* **283**, 301–310.
Huynh, K. K. & Grinstein, S. (2007). *Microbiol. Mol. Biol. Rev.* **71**, 452–462.
James, P., Isupov, M. N., Sayer, C., Saneei, V., Berg, S., Lioliou, M., Kotlar, H. K. & Littlechild, J. A. (2014). *Acta Cryst.* D**70**, 2607–2618.
Kabsch, W. (2010). *Acta Cryst.* D**66**, 133–144.
Krissinel, E. & Henrick, K. (2007). *J. Mol. Biol.* **372**, 774–797.
Kusters, J. G., van Vliet, A. H. M. & Kuipers, E. J. (2006). *Clin. Microbiol. Rev.* **19**, 449–490.
Liljas, A. & Laurberg, M. (2000). *EMBO Rep.* **1**, 16–17.
Lindskog, S. (1997). *Pharmacol. Ther.* **74**, 1–20.
Marcus, E. A., Moshfegh, A. P., Sachs, G. & Scott, D. R. (2005). *J. Bacteriol.* **187**, 729–738.
Modak, J. K., Revitt-Mills, S. A. & Roujeinikova, A. (2013). *Acta Cryst.* F**69**, 1252–1255.
Modakh, J. K., Liu, Y. C., Machuca, M. A., Supuran, C. T. & Roujeinikova, A. (2015). *PLoS One*, **10**, e0127149.
Nishimori, I., Minakuchi, T., Kohsaki, T., Onishi, S., Takeuchi, H., Vullo, D., Scozzafava, A. & Supuran, C. T. (2007). *Bioorg. Med. Chem. Lett.* **17**, 3585–3594.
Nishimori, I., Minakuchi, T., Morimoto, K., Sano, S., Onishi, S., Takeuchi, H., Vullo, D., Scozzafava, A. & Supuran, C. T. (2006). *J. Med. Chem.* **49**, 2117–2126.
Nishimori, I., Vullo, D., Minakuchi, T., Morimoto, K., Onishi, S., Scozzafava, A. & Supuran, C. T. (2006). *Bioorg. Med. Chem. Lett.* **16**, 2182–2188.
Suerbaum, S. & Michetti, P. (2002). *N. Engl. J. Med.* **347**, 1175–1186.
Supuran, C. T. (2011). *Front. Pharmacol.* **2**, 34.
Supuran, C. T. & Scozzafava, A. (2007). *Bioorg. Med. Chem.* **15**, 4336–4350.
Tripp, B. C., Smith, K. & Ferry, J. G. (2001). *J. Biol. Chem.* **276**, 48615–48618.
Vagin, A. & Teplyakov, A. (2010). *Acta Cryst.* D**66**, 22–25.
Vullo, D., Luca, V. D., Scozzafava, A., Carginale, V., Rossi, M., Supuran, C. T. & Capasso, C. (2013). *Bioorg. Med. Chem.* **21**, 1534–1538.
Wen, Y., Feng, J., Scott, D. R., Marcus, E. A. & Sachs, G. (2007). *J. Bacteriol.* **189**, 2426–2434.
Wen, Y., Marcus, E. A., Matrubutham, U., Gleeson, M. A., Scott, D. R. & Sachs, G. (2003). *Infect. Immun.* **71**, 5921–5939.
Winn, M. D. *et al.* (2011). *Acta Cryst.* D**67**, 235–242.
Zanotti, G. & Cendron, L. (2010). *IUBMB Life*, **62**, 715–723.